A Novel Method based on Long Short Term Memory Network and Discrete-Time Zeroing Neural Algorithm for Upper-Limb Continuous Estimation Using sEMG Signals

Yuanyuan Chai[1], Keping Liu[1,*] Chunxu Li[2], Zhongbo Sun[1], Long Jin,[3] Tian Shi[4]

1.Department of Control Engineering, Changchun University of Technology, Changchun 130012, PR China

2.Centre for Robotics and Neural Systems, University of Plymouth, Plymouth PL48AA, UK

3.School of information Science and Engineering, Lanzhou University, Lanzhou 730000, PR China

4.College of Communication Engineering, Jilin University, Changchun 130025, PR China

Abstract

In this paper, a novel closed-loop model based on surface electromyography (sEMG) comprised a long short term memory (LSTM) network and discrete-time zeroing neural algorithm called zeroing neural network (ZNN), which is developed to estimate joint angles and angular velocities of human upper limb with joint damping. The dynamic model of human upper limb with joint damping is set up as the initial equation.Then, the LSTM network is proposed as an open-loop model which described the input-output relationship between the sEMG signals and joint motion intention. Besides, a novel closed-loop model is built via ZNN for eliminating the predicted error of open-loop model and improving the accuracy of motion intention recognition. Founded on the sEMG signals, the continuous movement of human upper limb joint can be successfully estimated via the novel closed-loop model. The results show that for simple joint movements, the closed-loop model is able to estimate the movement intention of human upper limb with high accuracy.

Keywords: sEMG, LSTM network, Discrete-time zeroing neural algorithm,

[☆]The work is supported in part by the National Natural Science Foundation of China under Grant No. 61873304 and 51875047, and also in part by the China Postdoctoral Science Foundation Funded Project under Grant Nos. 2018M641784 and 2019T120240 and also in part by the Key Science and Technology Projects of Jilin Province, China, Grant No. 20200201291JC.

[*]Corresponding author.

E-mail addresses: liukeping@ccut.edu.cn (K. P. Liu).

1. Introduction

The bioelectric signal contains human behavior information, which could be used to identify human movement intentions. Thus, the effective human-machine interaction information was provided by bioelectric signals had been developed many applications in varies area. In medical area, a successful example was rehabilitation robots, which was able to improve actual movement of human-machine interaction and provide behavior prediction [1, 2, 3, 4]. At present, bioelectric signals mainly consisted of electromyography (EMG) [5], electroencephalogram (EEG) [6] and electrooculogram (EOG) [7]. Surface electromyography (sEMG) was a reliable way to recognize human motion intentions and could facilitate human-machine integration with the help of an intelligent machine perception system [8].

sEMG was a kind of non-stationary weak signals, when the muscle and its related motion unit was excited, the bioelectrical signals could be collects from the skin surface. The collection process was simple and non-invasive, making it a popular research field in human-machine interaction technology. At present, a fair amount of representative research on motion intention recognition based on sEMG has been reported, which can be broadly divided into two categories: classification of the motion pattern [9, 10, 11, 12, 13, 14] and estimation of the continuous motion of the joint [15, 16, 17, 18, 19]. Many classification methods applied continuous sEMG signals to estimate joint angles with predefined sets, such as support vector machine [9], artificial neural network [10], gaussian mixture model [11] and other classifiers [12, 13, 14]. Moreover, sEMG also could estimate the joint angle via Hill-type muscle model of human upper limb. In [15], the measurement equation established by the EMG function is exploited to extend the Hill-type muscle model to form a state-space model, and its able to reduce the model uncertainty and external interference. In addition, joint angle could be predicted via many neural network algorithms by their self-learning function, such as radial basis function (RBF) [16, 17], back propagation neural network (BPNN) [18] and convolutional neural network (CNN) [19]. In [17], a RBF neural network was used to predict the joint angle of healthy people. However, there was no experiment on spinal cord injury (SCI) patients. Furthermore, a nonlinear model based on BPNN was proposed to describe the sEMG signal and joint angle of human limb, which could be used for able-bodied subjects and SCI patients [18]. Compared with the traditional angle estimation method via sEMG signal, the nonlinear model in [18] had improved the estimation accuracy and real-time performance. Accordingly, the above neural networks were widely exploited to

predict joint angle founded on sEMG signals, and the experimental results also could be utilized to improve the rehabilitation of human limbs.

Among the most promising deep learning neural network algorithms, the long short term memory (LSTM) network became widely utilized in motion intention with long memory characteristics [20, 21, 22]. LSTM network was an excellent variant model of recurrent neural network (RNN), which could solve the problem of vanishing gradient caused by the gradual reduction of the gradient back propagation process. As for the motion intention recognition via sEMG, in motion classification, a pattern recognition model was presented that combined LSTM network with multilayer perceptron (MLP) for the feature learning and classification of sEMG signals. A feature space included the dynamic and static information of the sEMG signals was learnt by LSTM-MLP model, which improved the accuracy of motion classification [20]. In the field of estimation of continuous motion, a method was proposed for predicting motion intention of daily grasp movements by LSTM network [21]. Compared multiple methods, such as BPNN and RBF, LSTM network held the best performance for continuous estimation of grasp movement in that the LSTM network was able to eliminate gradient disappearance and gradient explosion during long sequence training. And in [21], it increased the estimation number of finger joint angles from 10 to 20. Furthermore, the LSTM network combined with other models could estimate intention identification of human body movement with better results. Combining the short connected auto encoder with the LSTM regression algorithm was developed to estimate continuous movement of shoulder and elbow joint angles based on sEMG signals [22]. However, these LSTM-based models had slight predicted errors, which had negative on influence human limbs rehabilitation. It is necessary to further research to eliminate the predicted errors. Therefore, a closed-loop model is utilized to eliminate the predicted errors.

Considering uncertain factors, such as physiological parameters, simplified models, measurement effect noise and external disturbance of traditional methods, they were invalid to estimate the continuous motion of upper limbs. However, overcoming these factors was essential for closed-loop systems. A strong convergence algorithm called zeroing neural network (ZNN) could lower the risks. It has exponential convergence and noise suppression capabilities, which was improved from RNN [23, 24, 25]. A comprehensive overview of the paper on ZNN was provided in [26], which was thoroughly described stability and analysed convergence of ZNN model. The core of the ZNN was to construct an error function, such as predicted errors of LSTM predicted model. Then, the information is exploited to make the error function to zero [27, 28, 29, 30].

In this paper, a neoteric method was proposed to estimate joint angles and angular

velocities of human upper limb with joint damping by using sEMG signals. The main intellectual contributions can be summarized as follows. The first objective is that a new continuous estimation approach combined LSTM network with ZNN as a closed-loop model is proposed, which can estimate the motion state of the human upper limb with joint damping. Second, for the uncertainty of the open-loop model, the ZNN method as a closed-loop feedback is exploited to eliminate the predicted error of open-loop model. Last, the effectiveness of LSTM-ZNN method as a closed-loop model needs to be testified founded on experimental results.

This paper consists of the following parts: Section 2 contains the acquisition and processing of experimental data. Following with the upper limb dynamic model and establishment of LSTM network model are introduced in Section 3. Section 4 introduces the formula of ZNN and the establishment of LSTM-ZNN model as a closed-loop model. In Section 5, based on analyzing the experimental results, the effectiveness of the closed-loop model is verified. Finally, Section 6 summarizes the achievements and predicts the future work.

2. Experimental

2.1. Data acquisition

In this paper, one healthy tester (female, 27 years old, 165cm, 55kg), without any history of neuromuscular disorder, has been selected to perform the required movements. The experiment is introduced in Fig.1, the equipments and sensors for signal acquisition are installed on the testers right upper limb to record EMG signals and joint angles while the upper limb in the process of flexion or extension. The signal acquisition equipment, which called Biopac, is exploited to acquire the sEMG signals, as presented in Fig.1. The device is a wireless physiological data acquisition and analysis system, which is able to record 10 sEMG data channels at the same time, with a sampling rate of 2k Hz for each channel. In this experiment, the sEMG signals are recorded of six selected types muscles of human upper limb via Biopac, which are anterior deltoid, posterior deltoid, biceps brachii, triceps brachii, extensor carpi radialis and flexor carpi radialis. In addition, the joint angle measuring device is manufactured by Wit Motion, as shown in Fig.1. Three sensors are attached to the human upper limb of the tester for collecting the angles of shoulder, elbow and wrist while in motion. As a result, the devices of data acquisition are input by the recorded joint angles and the sEMG signals of human upper limb.

It is important that keep clean of the test area, the skin surface need to be shaved if necessary. The uncleaned surface could increase the probability of distortion during the action [31]. A set of electrodes is attached to the skin surface, which is utilized

to measure the simulated sEMG signals. Each pair of electrodes is separated from each other with 2cm-3cm. The position of each electrode can also be found in Fig.1.

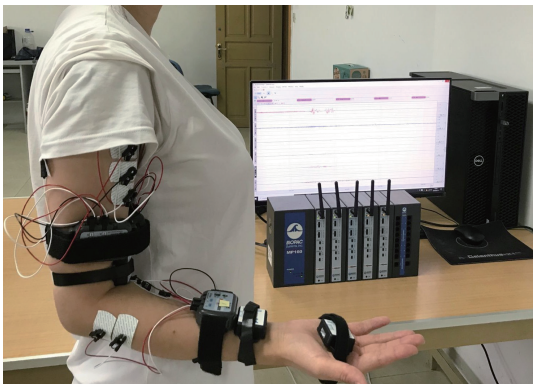

Fig. 1. Data acquisition experiment.

2.2. Signals processing

The raw sEMG signals are easily affected by noise during signal acquisition. The power density spectrum of sEMG presents that most of its power in the range from 5 Hz to 500 Hz. Therefore, the signal with high cutoff frequency of 500 Hz should be less considered. As considered above factors, the raw sEMG signals should be reduced the noise via a set of 50 Hz notch filter, 20 Hz low cut-off frequency filter and 500 Hz high-pass frequency bandpass filter. The sEMG signals need to be further digitized after removing the noise in the raw sEMG signals. Through the above steps, the raw sEMG signals and the preprocessed sEMG signals of six selected muscles are illustrated in Fig.2.

Moreover, the preprocessed sEMG signals are operated as follows. The waveform of the sEMG signals oscillates randomly in nature, and the signals vibrate very frequently around zero amplitude. The amplitude change can be more clearly observed via full-wave rectification. This process can be expressed as

$$\mathrm{sEMG}_r(n) = |\mathrm{sEMG}(n)| \tag{1}$$

where $\mathrm{sEMG}(n)$ is the nth amplitude of the signals after pretreatment, $\mathrm{sEMG}_r(n)$ is the nth amplitude sample of the sEMG signals obtained after full-wave rectification.

As the sampling frequency of signals are not consistent with the joint angle, sampling frequency of signals are 20 Hz and sampling frequency of the joint angle

is 100 Hz. The joint angle signal has much lower sampling frequency than sEMG signals. Therefore, to keep the consistency between two types of signals, the sEMG signals should be sub-sampled. The process can be introduced as

$$\mathrm{sEMG}_s(n) = \frac{1}{N} \sum_{i=nN-N+1}^{nN} \mathrm{sEMG}_r(i) \tag{2}$$

where N is the number of times that signals need to be sub-sampled, $\mathrm{sEMG}_s(n)$ is the sEMG signals after sub-sampling.

3. Open-loop model estimation

3.1. Establishment of upper limb dynamic model

Based on the anatomy, the human body is composed of bones, bone junctions and skeletal muscle. The bones connected to each other through joints, and therefore to form a hard human frame. Moreover, human upper limb consists of shoulder, upper arm, forearm and hand. There are a few important joints to link each part, such as sternoclavicular joint, shoulder joint, elbow joint, forearm bone connection and wrist joint. In this paper, only shoulder joint, elbow joint and wrist joint are considered to establish the three degrees of freedom (3–DOFs) dynamic model with joint damping of human upper limb, which is represented the relationship between joint angles, angular velocities and joint torque. The human upper limb skeleton diagram is displayed in Fig.3.

During the flexion and extension of the three joints, there would be resistance caused by the tissue near the three joints. It is called the joint damping M_p and can be described as

$$M_p = \frac{1}{2} P \dot{\theta}^2 \tag{3}$$

where P is the damping coefficient at each joint, $\dot{\theta}$ denotes the angular velocity.

The total torque rooted in dynamic model about the joints of upper limb is given as follows

$$M(\theta)\ddot{\theta} + C\left(\theta, \dot{\theta}\right)\dot{\theta} + G(\theta) + M_p = \tau_h \tag{4}$$

where θ and $\ddot{\theta}$ denote the joint angle and angular acceleration, M is the inertia matrix of the system, C is the centripetal-coriolis matrix, G is the gravity effects of upper arm, forearm and hand, τ_h is the joint torque.

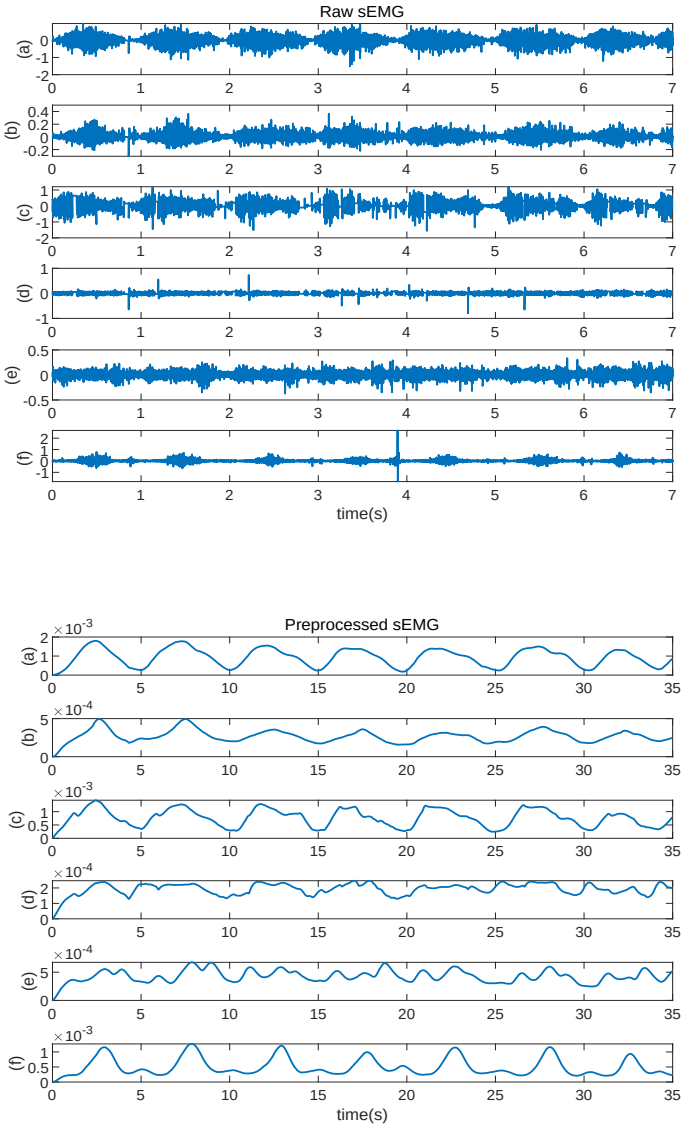

Fig. 2. Raw sEMG and preprocessed sEMG. (a)anterior deltoid; (b)posterior deltoid; (c)biceps brachii; (d)triceps brachii; (e)extensor carpi radialis; (f)flexor carpi radialis.

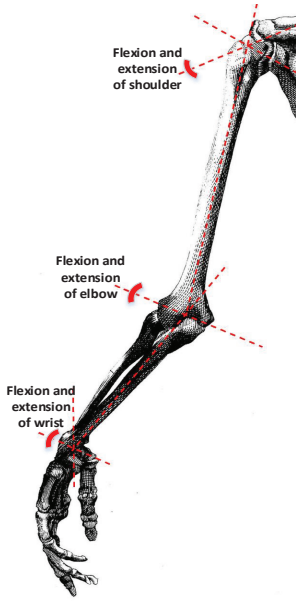

Fig. 3. Human upper limb skeleton diagram.

As the total torque acting on the joints is known, the angular and angular velocity of equation (4) can be reformulated as

$$\begin{cases} \dot{\theta}_1 = \theta_2 \\ \dot{\theta}_2 = -M^{-1}\left[C\left(\theta_1, \dot{\theta}_1\right)\dot{\theta}_1 + G(\theta_1) + \frac{1}{2}P\dot{\theta}_1^2\right] + M^{-1}\tau_h \end{cases} \tag{5}$$

where θ_1 and θ_2 are the joint angle and angular velocity respectively, which collected by Wit Motion sensors.

3.2. LSTM-based model

In this paper, the LSTM-based model aims to predict the joint angles and angular velocities with sEMG signals. Then, the predicted torque can be solved by predicted joint angles and angular velocities and equation (4).

In this experiment, the collected data of sEMG signals and joint angles and angular velocities are supposed as follows

$$\begin{cases} a_i = [a_{i,1}, \ldots, a_{i,t}] \\ b_h = [b_{h,1}, \ldots, b_{h,i}] \end{cases} \qquad t = 1, \ldots, j \tag{6}$$

where a_i is the sEMG signals of muscles measured by the Biopac, $b_h = [\theta_1; \theta_2]$, and j represents the number of muscles exploited in this experiment.

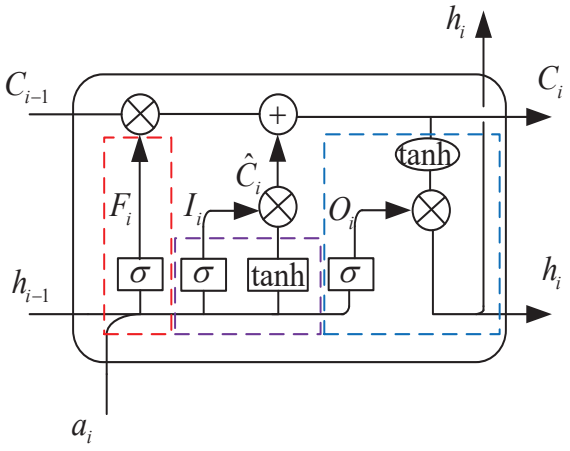

Fig. 4. The structure of LSTM network.

Considering the amplitude of sEMG signals has unique characteristics, which the contraction of muscles would cause the rise in amplitude. Moreover, the joint angles and angular velocities also change during the contraction. The relationship between them can be obtained by the following nonlinear functions

$$\begin{aligned} h_i = g\,(&a_{1,i}\,, \ldots, a_{1,i-m+1}; \\ &a_{2,i}, \ldots, a_{2,i-m+1}; \ldots; \\ &a_{k,i}, \ldots, a_{k,i-m+1};) \quad i = m, \ldots, t \end{aligned} \tag{7}$$

where $h_i = [\theta_{1,i}; \theta_{2,i}]$ is the joint angles and angular velocities estimated of three joints at the ith time, g is the undetermined nonlinear function, and m represents the order.

The LSTM network is build to estimate the relationship between the joint angles and angular velocities of three joints and sEMG signals. The internal state in the LSTM network is stored in a special unit to maintain a continuous error stream, therefore, the gradient neither explodes nor disappears in network. The control functions in a memory unit include save, write and read. The logic units do not send their inputs to other neurons. Thereby, the LSTM network has four network layers inside with a chain structure. Its repeating unit is different from the unit in a standard RNN with only one network layer. The structure of LSTM network is demonstrated in the Fig.4, which has three parts are called the forget gate, the input gate and the output gate.

The first step, or the forget gate, of the LSTM network is to decide whether the information needs to be discarded from the cell state or not. And this step follows

function as

$$F_i = \sigma\left(W_F h_{i-1} + V_F a_i\right) \tag{8}$$

where σ is the logistic sigmoid function, W_F and V_F are respectively recursive weight matrix and projection of input representation in forget gate.

Next step is deciding what new information should be added to the state of the cell in input gate. This step is obtained as follows

$$I_i = \sigma\left(W_I h_{i-1} + V_I a_i\right) \tag{9}$$

$$\hat{C}_i = \tanh\left(W_C h_{i-1} + V_C a_i\right) \tag{10}$$

where W_I and V_I are the recursive weight matrix and the projection of input representation in the input gate respectively. $\hat{C}_i$ is the new information of cell after tanh layer. W_C and V_C are state and projection weights of input respectively.

Then, old cell information C_{i-1} is updated to the new cell information C_i, which can be described as following equation

$$C_i = F_i \odot C_{i-1} + I_i \odot \hat{C}_i \tag{11}$$

where $\odot$ is a logical operator.

The final output of the LSTM unit is obtained as follows

$$O_i = \sigma\left(W_O h_{i-1} + V_O a_i\right) \tag{12}$$

$$h_i = O_i \odot \tanh\left(C_i\right) \tag{13}$$

where W_O and V_O are recursive weight matrix and projection of input representation in the output gate respectively.

There are six neurons in the input layer which represents the sEMG signals measured from anterior deltoid, posterior deltoid, biceps brachii, triceps brachii, extensor carpi radialis and flexor carpi radialis, and six neuron in the output layer which represents the joint angles and angular velocities of shoulder joint, elbow joint and wrist joint. The number of neurons in the hidden layer is uncertain. And the hidden layer has a great impact on the precision of elbow joint angle estimation. Moreover, the network performance is the key factor of the size of layers.

According to equation (4), the predicted total torque $\tau_{h,i}$ can be obtained

$$\tau_{h_i} = M\left(\theta_{1,i}\right)\ddot{\theta}_{1,i} + C\left(\theta_{1,i}, \theta_{2,i}\right)\theta_{2,i} + G\left(\theta_{1,i}\right) + \frac{1}{2}P{\theta_{2,i}}^2 \tag{14}$$

where $\theta_{1,i}$, $\theta_{2,i}$ and $\ddot{\theta}_{1,i}$ denote the predicted joint angles, angular velocities and angular accelerations.

Moreover, The predicted joint angles $\theta_{1,i}$ and angular velocities $\theta_{2,i}$ are rooted in the dynamic model, which can be described as follows

$$\begin{cases} \dot{\theta}_{1,i} = \theta_{2,i} \\ \dot{\theta}_{2,i} = -M^{-1}\left[C\left(\theta_{1,i}, \dot{\theta}_{1,i}\right)\dot{\theta}_{1,i} + G(\theta_{1,i}) + \frac{1}{2}P\dot{\theta}_{1,i}^{2}\right] + M^{-1}\tau_{h,i} \end{cases} \tag{15}$$

4. Closed-loop model estimation

The movement intention can be estimated by using the LSTM-based model (15), which is an open-loop control system. It is worthless that the inaccurate estimation due to the cumulative errors generated by suitable assumptions. Such as selecting training data sets to train the model which may cause the predicted errors increased in LSTM network and distortion of partially effective sEMG signals. As well as the intention recognition of subjects would be affected in the open-loop experiment.

As the open-loop model has no automatic correction capability, hence a closed-loop estimation method can be exploited to eliminate the influence of the accumulated errors, which is investigated for the motion intention of the human upper limb. In closed-loop systems, once the predicted joint angle deviates from the measured joint angle is detected, a corresponding control function will be generated to eliminate the deviation. Therefore, it is able to lower the interference and enhance the response characteristics of the system.

4.1. Zeroing neural network model

A nonlinear vector equation called zero-finding problem as described in [23, 25, 32], the zero-finding problem is considered as an example

$$f(x(t), t) = 0 \in R^{n}\ , t \subseteq [0, +\infty) \tag{16}$$

where $f : R^{n} \times [0, +\infty) \rightarrow R^{n}$ is a differential time-varying nonlinear mapping function. According to equation (16), $x(t) \in R^{n}$ is found as an objective in real time. For simplicity, a solution $x^{*}(t)$ of zero-finding problem is existed at any time instant $t \subseteq [0, +\infty)$. Hence, the time-varying error function $e(t) \in R^{n}$ can be written as follows

$$e(t) = f(x^{*}(t), t) - f(x(t), t) = 0 - f(x(t), t) \tag{17}$$

To keep time-varying error $e(t)$ near to zero, it is important to make $x(t)$ close to the time-varying state variable $x^{*}(t)$. Therefore, the zero-finding problem (16) can be described as a classical nonlinear dynamic system

$$\begin{cases} \dot{x} = u(t) \\ y(t) = f(x(t), t) = -e(t) \end{cases} \tag{18}$$

where $x(t)$ is the time-varying state variable of system, $u(t)$ and $e(t)$ respectively are time-varying control input function and output function.

Therefore, the classical nonlinear dynamic system (18) can be reformulated to find a controller $u(t)$ such that output variable $e(t)$ is regulated to zero. In addition, the time-varying error function $e(t)$ can be described as

$$\dot{e}(t) = -\gamma e(t) \tag{19}$$

where $\gamma > 0$ is a constant value, which is related to the rate of convergence. The formula means that $e(t)$ converges to zero with $\dot{e}(t)$ evolved along negative direction.

Theorem 1: (see [33]) The state variable $x(t)$ of classical nonlinear dynamic system (18) globally and exponentially converges to $x^*(t)$. Therefore, the control law can be designed as

$$u(t) = -\left(\frac{\partial f(x(t), t)}{\partial x}\right)^{-1} \left(\gamma \cdot f(x(t), t) + \frac{\partial f(x(t), t)}{\partial t}\right) \tag{20}$$

where $\partial f(x(t), t)/\partial t \in R^n$, besides, $\partial f(x(t), t)/\partial x(t) \in R^n \times R^n$ is nonsingular.
Proof:

Substituting (17) into (19) yields an implicit equation

$$J(x(t), t)\dot{x}(t) = -\gamma(f(x(t), t)) - \frac{\partial f(x(t), t)}{\partial t} \tag{21}$$

Substituting the equation (21) into the classical nonlinear dynamic system equation (18), the control law can be obtained as (20).

4.2. Discrete-time closed-loop estimation

Combining the LSTM-based model (15) with the classical nonlinear dynamic model (18), then the closed-loop model founded on ZNN model in discrete-time can be generalized as follows

$$\begin{cases} \theta_{k+1} = \theta_k + \dot{\theta}_k T_s \\ \dot{\theta}_{k+1} = f(\theta_k, t_k) + u(t_k) \end{cases} \tag{22}$$

where $\theta_k = [\theta_{i,k}; \dot{\theta}_{i,k}]$ is the time-varying state variable, T_s is the sampling time. The $f(\theta_k, t_k)$ is expressed as follows

$$f(\theta_k, t_k) = [\theta_{2,i,k}; -M^{-1}\left[C\left(\theta_{1,i,k}, \dot{\theta}_{1,i}\right)\dot{\theta}_{1,i,k} + G(\theta_{1,i,k}) + \frac{1}{2}P\dot{\theta}^2_{1,i,k}\right] + M^{-1}\tau_{i,k}] \tag{23}$$

According to the equation (20) and discrete-time technique, let $e(t_k) = \theta_{d,k} - \theta_k$, where $\theta_{d,k} = [\theta_1; \theta_2]$ in equation (5) is the desired state variable, the controller of the closed-loop model (22) can be obtained as

$$u_{ZNN}(t_k) = \dot{\theta}_{d,k} + \gamma(\theta_{d,k} - \theta_k) \tag{24}$$

The ZNN controller (24) can be deemed that provides a control framework for dealing with convergence and robustness issues of the discrete-time model . Moreover, closed-loop model (22) can improve the accuracy of motion intentions [23, 32]. Then, a comparative experiment of open-loop model and closed-loop model is conducted to verity the effectiveness of the proposed closed-loop model.

5. Experimental results and discussion

In order to verify the performances of the LSTM model (15) and LSTM-ZNN model (22), a structure of the system is explained in Fig.5, including its application to estimate the joint motion by using LSTM-ZNN model.

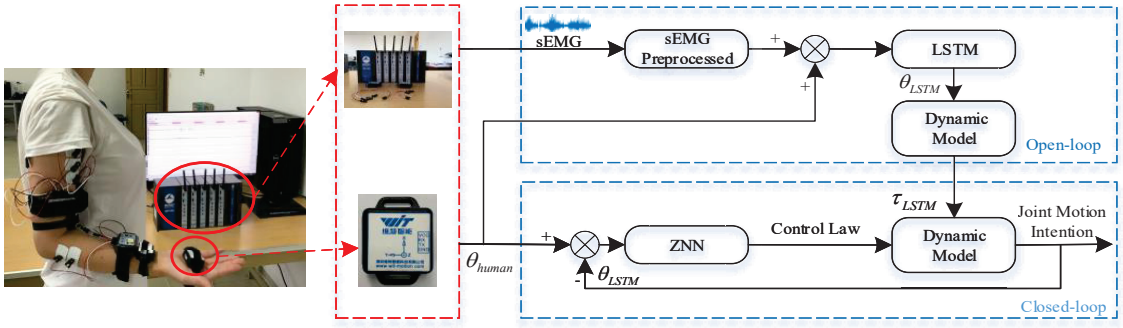

Fig. 5. Structure of motion intention recognition.

5.1. Open-loop model

By using the preprocessed sEMG signals of six selected muscles and three joint angles and angular velocities measured by sensors into the open-loop model, the LSTM network training algorithm is to estimate the motion states of human upper limb for continuous movements with sEMG measurements. According to equation (14), the predicted three joint torques of upper limb is shown in Fig.6.

In Fig.6, the green line indicates the experimental results of the estimated torques of open-loop model. And the blue line represents the actual value for three joint

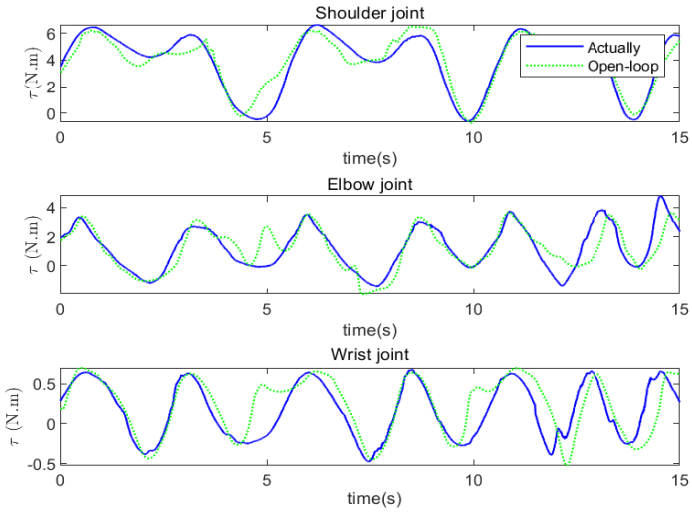

Fig. 6. Three joint torques of upper limb estimation with LSTM network.

torques which are calculated founded on the joint angles and angular velocities measured by sensors. It can be observed that the predicted torques of the three joints can be roughly close to the actual joint torques. In this experiment, due to the continuous movement of human upper limb, the three joint torques as outputs of the predicted network are not related to the current sEMG signals, but also related to their outputs in the past period of time. Therefore, the LSTM network holds the best performance for predicting motion intention in that the neurons of LSTM network are able to receive information from other neurons and their own information.

However, the results of torques are slightly diverged with actual torques, such as compared torques of three joints at time 5s and time 13s. Therefore, Fig.6 illustrates that open-loop model exists predicted errors while LSTM network in process. The predicted errors are existed because of the uncertainties in modeling process of the LSTM-based model. For instance, the number of neurons in the hidden layer of LSTM network is uncertain, which can impact on the precision of estimation. Furthermore, while performing the LSTM model to predict the joint angles and angular velocities, it needs notice that smaller training data sets can result in more errors. In addition, the motion intention rooted in open-loop model can be influenced by physiological characteristics, such as joint damping.

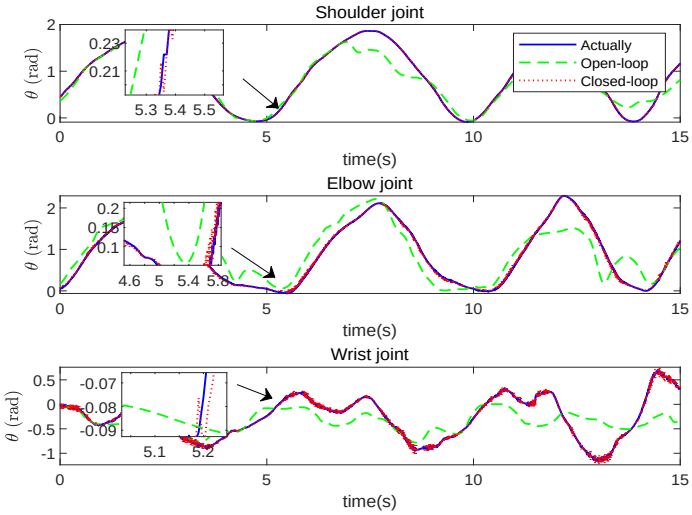

(a) Joint angle

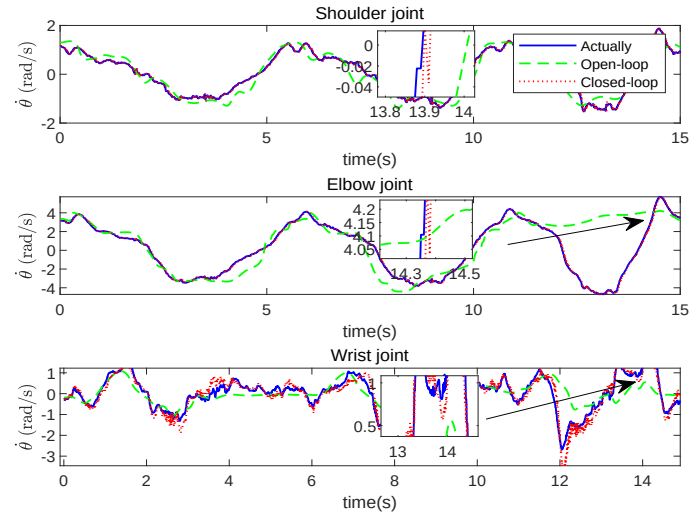

(b) Angular velocity

Fig. 7. Comparisons between the actually and estimation.

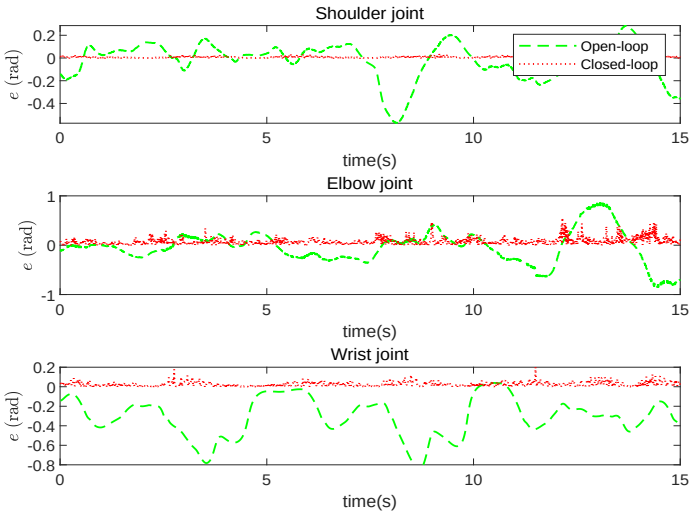

(a) Joint angle

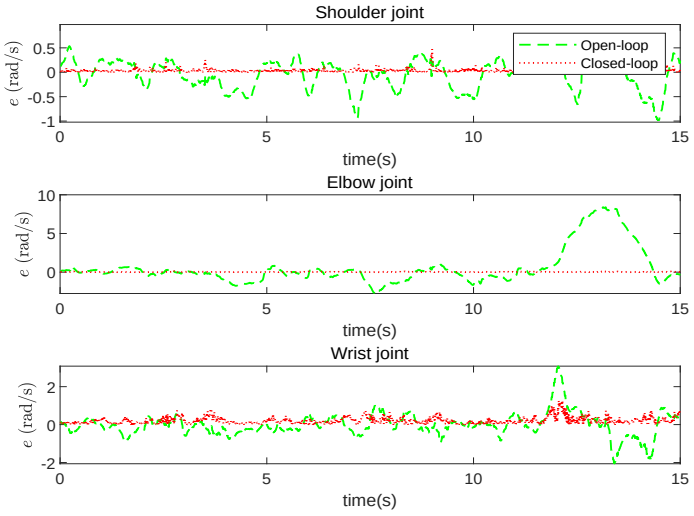

(b) Angular velocity

Fig. 8. Comparisons of error between the open-loop model and closed-loop model.

5.2. Closed-loop model

After training the LSTM network, the motion intention of human upper limb with joint damping is estimated by sEMG measurements. Then, the LSTM-ZNN model of equation (22) is utilized to reduce the predicted error. Moreover, the motion intention of the human upper limb with joint damping is estimated via closed-loop model. As a further step, the open-loop model is performed to verity the improvement of closed-loop model.

The actual joint angles and angular velocities measured by sensors are used to evaluate the performance of the open-loop and closed-loop models. Fig.7 illustrates the results of the open-loop model and the closed-loop model by using the sEMG data in Fig.2, where the blue lines are the measurements of the actual joint angles and angular velocities. It can be indicated that the predicted angles and angular velocities of open-loop model are quite similar to the actual values, but predicted errors exist. Such as the estimated joint angles of elbow joint and wrist joint of red line in Fig.7(a) at time 5s. The estimated joint angle of the shoulder joint is the red line in Fig.7(a), which exists slightly errors. As for the angular velocities, as shown in Fig.7(b), each line of the open-loop model deviates from the actual value, such as the estimated angular velocities of shoulder joint and wrist as red at time 4s, and at time 14s in estimation of the elbow joint.

Compared the predicted results of the open-loop and closed-loop model in Fig.7, the estimation performance is improved, which appeared the predicted value closer to the actual value by the LSTM-ZNN model. This is because that ZNN model (20) has strong robustness and high accuracy for the solution of time-varying nonlinear problem. In this paper, the estimated joint angles and angular velocities are regarded as the time-varying solution, which can converge to actual values founded on ZNN controller (24). Besides, the LSTM-ZNN model (22) has strong uncertainty rejection performance, which greatly reduces the influence brought by uncertain factors of the LSTM predicted model. Therefore, the closed-loop model holds the better performance for predicting joint angles and angular velocities in that the predicted errors of open-loop model are decreased founded on the ZNN controller (24).

Fig.8 signifies the experimental results of the estimation errors of angles and angular velocities with parameters $\gamma = 150$, where the green lines and red lines are the error between estimated angle and angular velocity by open-loop model and closed-loop model with the actual values respectively. In Fig.8, it can be shown that the the errors of predicted angles and angular velocities of open-loop model is larger than those of closed-loop model.

As observed the results in Fig.8, the experimental results show that the closed-loop model is obviously outperformed than the open-loop model. Because, the core

of the ZNN-based method is to construct an error function $e(t)$, and use information derived from $e(t)$ to force $\dot{e}(t)$ to zero as describe in equation (19). In this experiment, the predicted errors are regarded as an error function $e(t)$, which have been efficiently corrected by the LSTM-ZNN model. The performance indicates that the closed-loop model has convergence, which improves the accuracy of predicted results.

6. Conclusions

In this paper, a healthy female has completed the flexion and extension exercises of upper limb, which provides experimental data and reflects the conditions of the patients in reality. The relationship between the joint motion intention of upper limb with joint damping and sEMG signals has been verified by using LSTM network as an open-loop model in the measurements. Then, the predicted errors of open-loop model have been eliminated by the LSTM-ZNN model as a closed-loop model. By reason that the ZNN model has strong robustness and high accuracy for the solution of time-varying nonlinear problem. In this experiment, the novel closed-loop model is able to continuously capture the movement of human upper limb with joint damping. Moreover, the results also reveal that sEMG signals can be exploited to predict the angle and angular velocity with relatively high accuracy.

As a matter of fact, tremor movements are unable to predict due to the different individuals, which needs to be reduce the influence for the future tests. In addition, accurate and reliable acquisition of human motion intention is a prerequisite for application of human-machine interaction. After obtaining the movement intention of human, some control strategies are adopted to realize human-machine interaction control for spinal cord injury patients and stroke patients.

References

[1] K. X. Li, J. H. Zhang, L. F. Wang, M. L. Zhang, J. Y. Li, and S. C. Bao, A review of the key technologies for sEMG-based human-robot interaction systems, Biomedical Signal Processing and Control. 62(2020) 102074.

[2] J. T. Yang and C. Peng, Evolving control of human-exoskeleton system using Gaussian process with local model, Biomedical Signal Processing and Control. 58(2020) 101844.

[3] S. Z. Yang, and J. H. Zhang, An adaptive humanCmachine control system based on multiple fuzzy predictive models of operator functional state, Biomedical Signal Processing and Control. 8(2013) 302–310.

[4] Z. B. Sun, F. Li, Y. F. Lian, S. S. Liu, and K. P. Liu, An adaptive iterative learning control approach for lower limb rehabilitation robot in noisy environments, 2019 IEEE 9th Annual International Conference on CYBER Technology in Automation, Control, and Intelligent Systems. (2019) 905–910.

[5] R. Y. Ma, L. L. Z, G. F. Li, D. Jiang, S. Xu, and D. S. Chen, Grasping force prediction based on sEMG signals, Alexandria Engineering Journal. 59(2020) 1135–1147.

[6] L. D. Bai, J. Q. Guo, T. Y. Xu, and M. H. Yang, Emotional monitoring of learners based on EEG signal recognition, Procedia Computer Science. 174(2020) 364–368.

[7] G. Gallicchio, A. Cooke, and C. Ring, Assessing ocular activity during performance of motor skills using electrooculography, Psychophysiology. 55(2018) 1–12.

[8] L. Bi, A.G. Feleke, and C. Guan, A review on EMG-based motor intention prediction of continuous human upper limb motion for human-robot collaboration, Biomedical Signal Processing and Control. 51(2019) 113–127.

[9] J. J. A. M. Jnior, M. Freitas, H. Siqueira, A. E. Lazzaretti, S. Stevan and S. F. Pichorim, Comparative analysis among feature selection of sEMG signal for hand gesture classification by armband, IEEE Latin America Transactions. 18(2020) 1135–1143.

[10] S. M. Mane, A. Kambli, F. S. Kazi, and N. M. Singh, Hand motion recognition from single channel surface EMG using wavelet & artificial neural network, Procedia Computer Science. 49(2015) 58–65.

[11] Q. C. Ding, J. D. Han, X. G. Zhao, and Y. Chen, Missing-data classification with the extended full-dimensional gaussian mixture model: applications to EMG-based motion recognition, IEEE Transactions on Industrial Electronics. 62(2015) 4994–5005.

[12] S. H. Qi, X. M. Wu, W. H. Chen, J. M. Liu, J. B. Zhang, and J. H. Wang, sEMG-based recognition of composite motion with convolutional neural network, Sensors and Actuators A: Physical. 311(2020) 112046.

[13] J. K. Shao, Y. F. Niu, C. Q. Xue, Q. Wu, X. Z. Zhou, Y. Xi, and X. L. Zhao, Single-channel sEMG using wavelet deep belief networks for upper limb motion recognition, International Journal of Industrial Ergonomics. 76(2020) 102905.

[14] Y. Wang, Q. Wu, N. Dey, S. Fong, and A. S. Ashourg, Deep back propagation-Clong short-term memory network based upper-limb sEMG signal classification for automated rehabilitation, Biocybernetics and Biomedical Engineering. 40(2020) 987–1001.

[15] J. Han, Q. Ding, A. Xiong, and X. Zhao, A state-space EMG model for the estimation of continuous joint movements, IEEE Transactions on Industrial Electronics. 62(2015) 4267–4275.

[16] S. Wang, Y. Gao, J. Zhao, T. Yang and Y. Zhu, Prediction of sEMG-based tremor joint angle using the RBF neural network, 2012 IEEE International Conference on Mechatronics and Automation, Chengdu. (2012) 2103–2108.

[17] G. Wang, Y. B. Liu, T. Shi, X. Q. Duan, K. P. Liu, Z. B. Sun, and Long Jin, A novel estimation approach of sEMG-based joint movements via RBF neural network, 2019 Chinese Automation Congress (CAC), Hangzhou, China. (2019) 1783–1788.

[18] F. Zhang, P. F. Li, Z. G. Hou, Z. Lu, Y. X. Chen, Q. L. Li, and M. Tan, sEMG-based continuous estimation of joint angles of human legs by using BP neural network, Neurocomputing. 78(2012) 139–148.

[19] G. Liu, L. Zhang, B. Han, T. Zhang, Z. Wang, and P. Wei, sEMG-based continuous estimation of knee joint angle using deep learning with convolutional neural network, 2019 IEEE 15th International Conference on Automation Science and Engineering (CASE), Vancouver, BC, Canada. (2019) 140–145.

[20] Y. He, O. Fukuda, N. Bu, H. Okumura and N. Yamaguchi, Surface EMG pattern recognition using long short term memory combined with multilayer perceptron, 2018 40th Annual International Conference of the IEEE Engineering in Medicine and Biology Society (EMBC), Honolulu, HI. (2018) 5636-5639.

[21] C. Wang, W. Y. Guo, H. Zhang, L. L. Guo, C. C. Huang, and C. Lin, sEMG-based continuous estimation of grasp movements by long-short term memory network, Biomedical Signal Processing and Control. 59(2020) 101774.

[22] C. F. Ma, C. Lin, O. W. Samuel, L. S. Xu, and G.L. Li, Continuous estimation of upper limb joint angle from sEMG signals based on SCA-LSTM deep learning approach, Biomedical Signal Processing and Control. 61(2020) 102024.

[23] L. Jin, Y. N. Zhang, S. Li, and Y. Y. Zhang, Modified ZNN for timevarying quadratic programming with inherent tolerance to noises and its application to kinematic redundancy resolution of robot manipulators, IEEE Transactions on Industrial Electronice. 63(2016) 6978–6988.

[24] L. Jin, S. Li, B. Hu, M. Liu, and J. G. Yu, Noise-suppressing neural algorithm for solving time-varying system of linear equations: a controlbased approach, IEEE Transactions on Industrial Informatics. 15(2019) 236–246.

[25] L. Jin, S. Li, and B. Hu, RNN models for dynamic matrix inversion: a control-theoretical perspective, IEEE Transactions on Industrial Informatics. 14(2018) 189–199.

[26] L. Jin, S. Li, B. L. Liao, and Z. J. Zhang, Zeroing neural network: a survey, Neurocomputing. 267(2017) 597–604.

[27] L. Jin, Z. T. Xie, M. Liu, K. Chen, C. X. Li, and C. G. Yang, Novel joint-drift-free scheme at acceleration level for robotic redundancy resolution with tracking error theoretically eliminated, IEEE/ASME Transactions on Mechatronics. In Press with DOI: 10.1109/TMECH.2020.3001624.

[28] Z. T. Xie, L. Jin, X. Luo, Z. B. Sun, and M. Liu, RNN for repetitive motion generation of redundant robot manipulators: an orthogonal projection-based scheme, IEEE Transactions on Neural Networks and Learning Systems. In Press with DOI: 10.1109/TNNLS.2020.3028304.

[29] L. Wei, L. Jin, C. G. Yang, K. Chen, and W. B. Li, New noise-tolerant neural algorithms for future dynamic nonlinear optimization with estimation on hessian matrix inversion, IEEE Transactions on Systems, Man, and Cybernetics: Systems. In Press DOI: 10.1109/TSMC.2019.2916892.

[30] L. Jin, J. K. Yan, X. J. Du, X. C. Xiao, and D. Y. Fu, RNN for solving time-variant generalized sylvester equation with applications to robots and acoustic source localization, IEEE Transactions on Industrial Informatics. In Press DOI: 10.1109/TII.2020.2964817.

[31] B. U. Kleine, D. F. Stegeman, and D. Mund, Influence of motoneuron firing synchronization on SEMG characteristics in dependence of electrode position, Journal of Applied Physiology. 91(2001) 1588–1599.

[32] Z. B. Sun, T. Shi, L. Wei, Y. Y. Sun, K. P. Liu, and L. Jin, Noise-suppressing zeroing neural network for online solving timevarying nonlinear optimization problem: a control-based approach, Neural Computing and Applications. 32(2020) 11505–11520.

[33] L. Jin, Y. Zhang, S. Li, and Y. Zhang, Noise-tolerant ZNN models for solving time-varying zero-finding problems: A control-theoretic approach, IEEE Transactions on Automatic Control. 62(2017) 992–997.